Inorg. Chem. **2007**, *46*, 5585–5590

Effects of Isovalent Substitution in the Manganese Sublattice on Magnetic, Thermal, and Structural Properties of $BiMnO_3$: $BiMn_{1-x}M_xO_3$ ($M = Al, Sc, Cr, Fe, Ga$; $0 \leq x \leq 0.2$)

Alexei A. Belik* and Eiji Takayama-Muromachi

Advanced Nano Materials Laboratory (ANML), National Institute for Materials Science (NIMS), 1-1 Namiki, Tsukuba, Ibaraki 305-0044, Japan

Received January 30, 2007

Solid solutions $BiMn_{1-x}M_xO_3$ with M = Al, Sc, Cr, Fe, and Ga and $0 \leq x \leq 0.2$ were prepared at a high pressure of 6 GPa and 1333–1453 K, and their magnetic, thermal, and structural properties were investigated. The orbital-ordered monoclinic phase of $BiMnO_3$ (phase I) is destroyed by a small percentage of substitution. The M elements can be classified by their ability to destroy phase I in the sequence Ga ($x \approx 0.08$) ≈ Fe ($x \approx 0.08$) < Cr ($x \approx 0.04$) ≈ Al ($x \approx 0.04$) < Sc ($x \approx 0.02$), where phase I is most stable for Ga substitution (up to $x \approx 0.08$) and less stable for Sc substitution (up to $x \approx 0.02$). The orbital-disordered high-temperature monoclinic phase of $BiMnO_3$ (phase II) is stabilized with larger *x*. In all cases, a compositional range was found where phases I and II coexist at room temperature. In phase I, the effect of substitution on the ferromagnetic transition temperature is weak (e.g., T_C = 102 K for $BiMnO_3$ and T_C = 99 K for $BiMn_{0.95}Ga_{0.05}O_3$), but there is a drastic effect on the orbital ordering temperature (e.g., T_{OO} = 474 K for $BiMnO_3$ and T_{OO} = 412 K for $BiMn_{0.95}Ga_{0.05}O_3$). Magnetic susceptibilities of phase I are typical for ferromagnets while, in phase II, ferromagnetic cluster-glass-like behavior is observed. The magnetic transition temperature of phase II (e.g., T_C = 70 K for $BiMn_{0.8}Ga_{0.2}O_3$) exhibits a sudden drop compared with that of phase I. The effect of substitution on the structural monoclinic-to-orthorhombic transition is different depending on M (e.g., T_{str} = 768 K for $BiMnO_3$, T_{str} = 800 K for $BiMn_{0.95}Ga_{0.05}O_3$, and T_{str} = 738 K for $BiMn_{0.85}Cr_{0.15}O_3$).

Introduction

Mutriferroics are an interesting class of materials from viewpoints of application and basic physics.[1−6] In multiferroics, two or all three of (anti)ferroelectricity, (anti)ferromagnetism, and ferroelasticity are observed in the same phase.[1] The first interest to these materials was in 1960−1970.[7−9] However at that time, they did not attract much attention because of difficulties in preparation of good samples and very weak coupling between different order parameters. Mutriferroics have experienced revival interest in the recent years[6] because of the advanced preparation and characterization techniques.[2]

$BiMnO_3$ was first prepared and characterized in 1960s.[7,8] Its ferromagnetic properties are well established with the ferromagnetic Curie temperature of 99−103 K.[7,10−12] After publications on the crystal structure determination of $BiMnO_3$ in noncetrosymmetric space group $C2$[13] and theoretical and experimental evidence for the likely occurrence of magnetoferroelectricity,[11,14] $BiMnO_3$ has been extensively studied as a multiferroic material.[12,15−26] Thin film samples of $BiMnO_3$ show promising results for practical applications.[16−18] Orbital

* To whom correspondence should be addressed. E-mail: Alexei.BELIK@nims.go.jp.

(1) Hill, N. A. *J. Phys. Chem. B* **2000**, *104*, 6694.
(2) Ramesh, R.; Spaldin, N. A. *Nat. Mater.* **2007**, *6*, 21.
(3) Cheong, S.-W.; Mostovoy, M. *Nat. Mater.* **2007**, *6*, 13.
(4) Eerenstein, W.; Mathur, N. D.; Scott, J. F. *Nature* **2006**, *442*, 759.
(5) Khomskii, D. I. *J. Magn. Magn. Mater.* **2006**, *306*, 1.
(6) Fiebig, M. *J. Phys. D: Appl. Phys.* **2005**, *38*, R123.
(7) Sugawara, F.; Iiida, S.; Syono, Y.; Akimoto, S. *J. Phys. Soc. Jpn.* **1968**, *25*, 1553.
(8) Tomashpol'fskii, Y. Y.; Zubova, E. V.; Burdina, K. P.; Venevtsev, Y. N. *Inorg. Mater.* **1967**, *3*, 1861.
(9) Smolenskii, G. A.; Chupis, I. E. *Sov. Phys. Usp.* **1982**, *25*, 475.
(10) Moreira dos Santos, A.; Cheetham, A. K.; Atou, T.; Syono, Y.; Yamaguchi, Y.; Ohoyama, K.; Chiba, H.; Rao, C. N. R. *Phys. Rev. B* **2002**, *66*, 064425.
(11) dos Santos, A. M.; Parashar, S.; Raju, A. R.; Zhao, Y. S.; Cheetham, A. K.; Rao, C. N. R. *Solid State Commun.* **2002**, *122*, 49.
(12) Kimura, T.; Kawamoto, S.; Yamada, I.; Azuma, M.; Takano, M.; Tokura, Y. *Phys. Rev. B* **2003**, *67*, 180401(R).
(13) Atou, T.; Chiba, H.; Ohoyama, K.; Yamaguchi, Y.; Syono, Y. *J. Solid State Chem.* **1999**, *145*, 639.
(14) Seshadri, R.; Hill, N. A. *Chem. Mater.* **2001**, *13*, 2892.
(15) Shishidou, T.; Mikamo, N.; Uratani, Y.; Ishii, F.; Oguchi, T. *J. Phys.: Condens. Matter* **2004**, *16*, S5677.

10.1021/ic0701615 CCC: $37.00
Published on Web 06/12/2007

degrees of freedom are also active in $BiMnO_3$ similar to $LaMnO_3$ as found by resonant X-ray scattering studies.[24] Therefore, different order parameters exist in $BiMnO_3$ and make it quite interesting.

$BiMnO_3$ undergoes two high-temperature phase transitions at 474 and 768 K.[8,12,20−22,26] The phase transition at 474 K is monoclinic-to-monoclinic. The low-temperature monoclinic phase (phase I) is characterized by the monoclinic β angle of about 110°, and the high-temperature monoclinic phase (phase II) has the β of about 108°.[12,22,26] Structure analysis of $BiMnO_3$ at 300 and 550 K using high-resolution neutron powder diffraction allowed us to suggest that the monoclinic-to-monoclinic transition corresponds to the orbital melting.[26] The phase transition at 768 K is monoclinic-to-orthorhombic.[12,22]

Heterovalent substitutions in the Bi sublattice of $BiMnO_3$ have been investigated in a number of works. Transitions with different spin, charge, and orbital orders were found in $Bi_{1-x}M_xMnO_3$ (M = Ca and Sr).[27,28] While different substitutions in both sublattices have been studied in $LaMnO_3$,[29−31] there is no information, to the best of our knowledge, on substitution effects in the Mn sublattice of bulk $BiMnO_3$. We have recently investigated solid solutions $BiMn_{1-x}Sc_xO_3$ in the whole compositional range and found that the orbital order in $BiMnO_3$ is destroyed by the 5% substitution of Sc for Mn.[32] The temperature of the magnetic transitions decreases and the temperature of the structural monoclinic-to-orthorhombic phase transition increases with increasing x in $BiMn_{1-x}Sc_xO_3$. The evolution of magnetic ground states was also proposed.

In this work, we focused on the systematic studies of effects of isovalent substitution (up to 20%) in the Mn sublattice of $BiMnO_3$ on the magnetic, orbital-order, and structural phase transitions. We have found that less than 10% of substitution destroys the orbital-ordered phase I in $BiMn_{1-x}M_xO_3$ (M = Al, Sc, Cr, Fe, Ga). In addition, phases I and II have different magnetic properties. Note that the $BiCrO_3$[33] and $BiScO_3$[34] end members of solid solutions $BiMn_{1-x}M_xO_3$ are isostructural with $BiMnO_3$ and adopt the phase II structure. $BiAlO_3$[35] and $BiFeO_3$[36] are perovskite oxides crystallizing in space group $R3c$, and $BiGaO_3$ is a pyroxene-type oxide.[35]

Experimental Section

Stoichiometric mixtures of Bi_2O_3 (99.99%), M_2O_3 (M = Al, Sc, Cr, Fe, Ga; 99.9%), and Mn_2O_3 were placed in Au capsules and treated at 6 GPa in a belt-type high-pressure apparatus at 1443−1453 K (M = Al, Sc, Cr, Ga), 1383 K (M = Fe and $x = 0.05$), and 1333 K (M = Fe and $x = 0.1$ and 0.15) for 60−70 min. After heat treatment the samples were quenched to room temperature (RT), and the pressure was slowly released. The resultant samples were black powders. X-ray powder diffraction (XRD) showed that some samples contained a very small amount of $Bi_2O_2CO_3$ as an impurity in addition to perovskite phases. Single-phased Mn_2O_3 was prepared from a commercial MnO_2 (99.99%) by heating in air at 923 K for 24 h. Note that strong reaction of the $BiMn_{1-x}Fe_xO_3$ system with Au capsules was found when high synthesis temperature was used (1443 K).

Magnetic susceptibilities, $\chi = M/H$, of $BiMn_{1-x}M_xO_3$ were measured on a SQUID magnetometer (Quantum Design, MPMS) between 2 and 300 K in an applied field of 100 Oe under both zero-field-cooled (ZFC) and field-cooled (FC) conditions. Isothermal magnetization measurements were performed between −50 and 50 kOe at 5 K.

Differential scanning calorimetry (DSC) curves of $BiMn_{1-x}M_xO_3$ were recorded on a SII Exstar 6000 (DSC 6220) system at a heating/cooling rate of 10 K/min from 133 K to maximum 873 K in semi-closed aluminum capsules. Each sample was heated above ∼20−50 K from the peak position observed above 740 K. The DSC runs of the samples containing monoclinic phase I were cycled between 150 and 520 K several times, then the samples were heated above 740 K, and finally the DSC runs were cycled again between 150 and 520 K.

XRD data of $BiMn_{1-x}M_xO_3$ were collected at RT on a RIGAKU Ultima III diffractometer using Cu Kα radiation (2θ range of 8−80°, a step width of 0.02°, and a counting time of 1 s/step). The XRD data were analyzed by the Rietveld method with RIETAN-2000.[37]

Results and Discussion

The lattice parameters were refined by the Rietveld method adopting the $C2/c$ model[26,32,34] and summarized in Table 1. In all the systems, there is a compositional range where two monoclinic phases (phases I and II) coexist. For example in the $BiMn_{1-x}Cr_xO_3$ system, the samples with $x = 0.05$ and 0.1 were mixtures of phases I and II with different fractions.

(16) Sharan, A.; Lettieri, J.; Jia, Y.; Tian, W.; Pan, X.; Schlom, D. G.; Gopalan, V. *Phys. Rev. B* **2004**, *69*, 214109.
(17) Son, J. Y.; Kim, B. G.; Kim, C. H.; Cho, J. H. *Appl. Phys. Lett.* **2004**, *84*, 4971.
(18) Gajek, M.; Bibes, M.; Barthelemy, A.; Bouzehouane, K.; Fusil, S.; Varela, M.; Fontcuberta, J.; Fert, A. *Phys. Rev. B* **2005**, *72*, 020406.
(19) Eerenstein, W.; Morrison, F. D.; Scott, J. F.; Mathur, N. D. *Appl. Phys. Lett.* **2005**, *87*, 101906.
(20) Chi, Z. H.; Xiao, C. J.; Feng, S. M.; Li, F. Y.; Jin, C. Q.; Wang, X. H.; Chen, R. Z.; Li, L. T. *J. Appl. Phys.* **2005**, *98*, 103519.
(21) Montanari, E.; Righi, L.; Calestani, G.; Migliori, A.; Gilioli, E.; Bolzoni, F. *Chem. Mater.* **2005**, *17*, 1765.
(22) Montanari, E.; Calestani, G.; Migliori, A.; Dapiaggi, M.; Bolzoni, F.; Cabassi, R.; Gilioli, E. *Chem. Mater.* **2005**, *17*, 6457.
(23) Yang, C. H.; Koo, T. Y.; Lee, S. H.; Song, C.; Lee, K. B.; Jeong, Y. H. *Europhys. Lett.* **2006**, *74*, 348.
(24) Yang, C. H.; Koo, J.; Song, C.; Koo, T. Y.; Lee, K. B.; Jeong, Y. H. *Phys. Rev. B* **2006**, *73*, 224112.
(25) Belik, A. A.; Takayama-Muromachi, E. *Inorg. Chem.* **2006**, *45*, 10224.
(26) Belik, A. A.; Iikubo, S.; Yokosawa, T.; Kodama, K.; Igawa, N.; Shamoto, S.; Azuma, M.; Takano, M.; Kimoto, K.; Matsui, Y.; Takayama-Muromachi, E. *J. Am. Chem. Soc.* **2007**, *129*, 971.
(27) Goff, R. J.; Attfield, J. P. *J. Solid State Chem.* **2006**, *179*, 1369.
(28) (a) Troyanchuk, I. O.; Mantytskaya, O. S.; Chobot, A. N. *Phys. Solid State* **2002**, *44*, 2266. (b) Woo, H.; Tyson, T. A.; Croft, M.; Cheong, S. W.; Woicik, J. C. *Phys. Rev. B* **2001**, *63*, 134412. (c) Hervieu, M.; Maignan, A.; Martin, C.; Nguyen, N.; Raveau, B. *Chem. Mater.* **2001**, *13*, 1356.
(29) (a) Zhou, J. S.; Goodenough, J. B. *Phys. Rev. B* **2003**, *68*, 144406. (b) Zhou, J. S.; Yin, H. Q.; Goodenough, J. B. *Phys. Rev. B* **2001**, *63*, 184423. (c) Goodenough, J. B.; Dass, R. I.; Zhou, J. S. *Solid State Sci.* **2002**, *4*, 297.
(30) Blasco, J.; Garcia, J.; Campo, J.; Sanchez, M. C.; Subias, G. *Phys. Rev. B* **2002**, *66*, 174431.
(31) Van Aken, B. B.; Jurchescu, O. D.; Meetsma, A.; Tomioka, Y.; Tokura, Y.; Palstra, T. T. M. *Phys. Rev. Lett.* **2003**, *90*, 066403.
(32) Belik, A. A.; Yokosawa, T.; Kimoto, K.; Matsui, Y.; Takayama-Muromachi, E. *Chem. Mater.* **2007**, *19*, 1679.
(33) Niitaka, S.; Azuma, M.; Takano, M.; Nishibori, E.; Takata, M.; Sakata, M. *Solid State Ionics* **2004**, *172*, 557.
(34) Belik, A. A.; Iikubo, S.; Kodama, K.; Igawa, N.; Shamoto, S.; Maie, M.; Nagai, T.; Matsui, Y.; Stefanovich, S. Yu.; Lazoryak, B. I.; Takayama-Muromachi, E. *J. Am. Chem. Soc.* **2006**, *128*, 706.
(35) Belik, A. A.; Wuernisha, T.; Kamiyama, T.; Mori, K.; Maie, M.; Nagai, T.; Matsui, Y.; Takayama-Muromachi, E. *Chem. Mater.* **2006**, *18*, 133.

Table 1. Lattice Parameters of $BiMn_{1-x}M_xO_3$[a]

M	*x*	fractn (%)	*a* (Å)	*b* (Å)	*c* (Å)	*β* (deg)	*V* (Å^3)
	0[26]	100	9.5415(2)	5.61263(8)	9.8632(2)	110.658(1)	494.24(2)
Al	0.03	100	9.5255(3)	5.6035(2)	9.8410(4)	110.458(3)	492.14(3)
Al	0.10	100	9.5073(3)	5.5810(2)	9.7118(3)	108.738(3)	487.99(3)
Sc	**0.01**	100	9.5397(3)	5.61286(14)	9.8603(3)	110.616(3)	494.16(2)
Sc	*0.05**	3	9.5397	5.61286	9.8603	110.616	494.16
	0.05[32]	97	9.5857(3)	5.5972(2)	9.7604(2)	108.899(2)	495.44(2)
Sc	0.10[32]	100	9.6029(3)	5.60988(14)	9.7690(3)	108.775(2)	498.26(2)
Cr	**0.03**	100	9.5333(4)	5.6080(2)	9.8502(4)	110.497(4)	493.28(4)
Cr	*0.05**	88	9.5299(3)	5.60598(13)	9.8450(3)	110.400(2)	492.98(2)
	0.05	12	9.5305	5.5893	9.7408	108.773	491.27
Cr	*0.10**	8	9.5299	5.60598	9.8450	110.400	492.98
	0.10	92	9.5305(4)	5.5893(2)	9.7408(4)	108.773(3)	491.27(3)
Cr	0.15	100	9.5099(4)	5.5858(2)	9.7238(3)	108.617(3)	489.50(3)
Fe	**0.05**	100	9.5355(3)	5.6103(2)	9.8530(3)	110.474(2)	493.81(3)
Fe	*0.10**	62	9.5269(4)	5.6095(2)	9.8381(4)	110.165(3)	493.54(3)
	0.10	38	9.5417(6)	5.6009(3)	9.7476(6)	108.792(5)	493.16(5)
Fe	0.15	100	9.5347(3)	5.6045(2)	9.7403(3)	108.674(3)	493.10(3)
Ga	**0.05**	100	9.5297(3)	5.60869(14)	9.8478(3)	110.453(3)	493.18(2)
Ga	*0.10**	65	9.5202(4)	5.6062(2)	9.8323(4)	110.210(3)	492.46(4)
	0.10	35	9.5306(8)	5.5997(4)	9.7347(7)	108.678(7)	492.16(6)
Ga	0.20	100	9.4963(4)	5.6033(2)	9.7065(4)	108.414(4)	490.04(3)
Cr[b]	0.15	100	9.5111(5)	5.5852(2)	9.7170(5)	108.573(5)	489.29(4)
Fe[b]	**0.05**	100	9.5268(4)	5.6123(2)	9.8376(5)	110.249(4)	493.48(4)
Ga[b]	**0.05**	100	9.5265(4)	5.6085(2)	9.8371(5)	110.320(4)	492.88(4)

[a] The lattice parameters without standard deviations were fixed during the refinement. The compositions marked by bold *x* are in the orbital-ordered state (phase I); the compositions marked by italic *x* contained two phases (I (asterisked) and II). [b] After the DSC experiments up to the maximum temperature T_{max} (see Table 2).

Table 2. Thermal Properties of $BiMn_{1-x}M_xO_3$ from the DSC Curves[a]

M	*x*	T_{OO} (K) of I	peak area at T_{OO} (J/g)	T_{str} or T_{dec} (K)	T_{max} (K) of DSC	phase composn after DSC by XRD
	0[26]	474	4.5	768	790	phase I
Al	**0.03**	390	1.8	780	810	pd: phases I and II + $Bi_{12}MnO_{20}$ (~6%)
Al	0.10	-	-	783	830	phase II
Sc	**0.01**	449	3.7	760	790	pd: phase I + Bi_2O_3 (~10%)
Sc	*0.05*[32]	- -	-	765	821	phase II
Sc	0.10[32]	-	-	779	826	phase II
Cr	**0.03**	425	2.9	758, 764	823	pd: phase I + Bi_2O_3 (~10%)
Cr	*0.05*	395	-	760	800	pd: phases I and II + $Bi_{12}MnO_{20}$ (<1%)
Cr	0.15	-	-	738	790	phase II
Fe	**0.05**	414	2.4	779	795	phase I
Fe	*0.10*	317	-	800	820	phases I and II
Fe	0.15	-	-	789, 796, 811	850	pd: phase II + Bi_2O_3 + ?
Ga	**0.05**	412	2.5	800	823	phase I
Ga	*0.10*	313	-	705,[b] 788[b]	833	d: Bi_2O_3 + $Bi_{12}MnO_{20}$ +?
Ga	0.20	-	-	860[b]	873	d: $Bi_2Mn_4O_{10}$ + $Bi_{12}MnO_{20}$

[a] The compositions marked by bold *x* are in the orbital-ordered state (phase I); the compositions marked by italic *x* contained two phases (I and II). T_{OO} is given for phase I in the single-phased and two-phased samples, but the peak area at T_{OO} is given for samples containing the only phase I. T_{str} or T_{dec} give the position of peaks on the DSC curves observed above 740 K. T_{max} is the maximum temperature of heating in the DSC experiments. Key: "-" means the parameters are not determined; "- -" means out of detection limit; "pd" is the partial decomposition; "d" is the decomposition of the sample; "?" means that there were additional unidentified reflections on XRD patterns. [b] Exothermal peaks.

Note that mass percentages of phases given in Table 1 were calculated from the refined scale factors in the Rietveld analyses. The amount of phases I and II in samples with the nominal compositions of $BiMn_{0.9}Fe_{0.1}O_3$ and $BiMn_{0.9}Ga_{0.1}O_3$ was comparable. Therefore, the lattice parameter could be refined for both phases. In other samples with small amount of one phase, the lattice parameters of the minor phase were fixed and not refined. The dependence of the lattice parameters on composition in the $BiMn_{1-x}Fe_xO_3$ and $BiMn_{1-x}Ga_xO_3$ systems is given in Figure 1. In these two systems, the lattice parameters change quite similarly with *x*. There are sudden jumps of the lattice parameters on the transition from phase I to phase II.

The M elements can be classified by their ability to destroy phase I in the sequence Ga ($x \approx 0.08$) ≈ Fe ($x \approx 0.08$) < Cr ($x \approx 0.04$) ≈ Al ($x \approx 0.04$) < Sc ($x \approx 0.02$), where phase I is most stable for Ga substitution (up to $x \approx 0.08$) and less stable for Sc substitution (up to $x \approx 0.02$). In all the cases, less than 10% of substitution destroys the orbital-ordered phase I of $BiMnO_3$. The orbital order of $BiMnO_3$ is less stable to the substitution in the Mn sublattice than that of $LaMnO_3$. For example, the orbital order disappears in $LaMn_{1-x}Ga_xO_3$ only for $x > 0.4$.[29,30] This fact can be explained by the presence of frustrated magnetic interactions in $BiMnO_3$ compared with unfrustrated interaction pattern in $LaMnO_3$.[23−26,32]

Figure 2 depicts the DSC curves of $BiMn_{1-x}M_xO_3$ (adopting the phase I structure) in the vicinity of the orbital order transition. Even a very small amount of substitution in the Mn sublattice has a drastic effect on the orbital ordering tem-

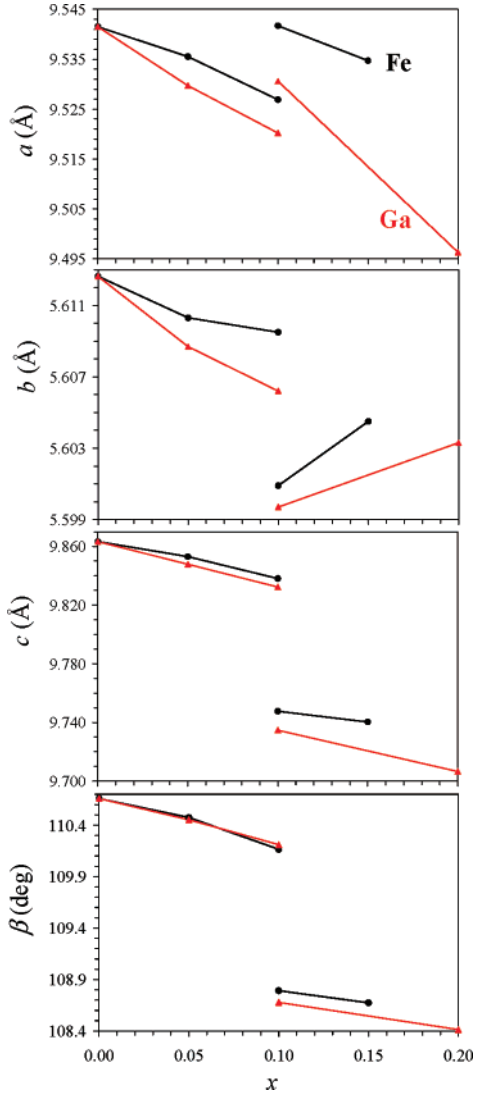

Figure 1. Dependence of the lattice parameters of $BiMn_{1-x}Fe_xO_3$ and $BiMn_{1-x}Ga_xO_3$ ($0 \le x \le 0.2$) on the composition.

perature (T_{OO}). For example, T_{OO} decreases from 474 K in $BiMnO_3$ to 449 K in $BiMn_{0.99}Sc_{0.01}O_3$ and 390 K in $BiMn_{0.97}Al_{0.03}O_3$ (Table 2). The width of the DSC peaks noticeable increases, and the peak area decreases with increasing x. These results show that orbital order in $BiMnO_3$ is very fragile. The cycling of the DSC runs for the as-prepared samples below 520 K gave reproducible results with the same peak positions and intensities (see Supporting Information).

Figure 3 shows the DSC curves of some samples measured up to high temperatures. After the DSC experiments, the phase composition of samples was checked by XRD, and the results are summarized in Table 2. Some samples decomposed partially or completely. The partially decomposed samples showed additional weak anomalies on the DSC curves near 700 K (see Supporting Information). The $BiMn_{0.8}Ga_{0.2}O_3$ sample decomposed completely. This sample showed a strong exothermal peak at 860 K and weigh gain of about 0.15% (the sample weight was measured before and after the DSC experiments).

Other samples kept their original structure and phase composition after the DSC experiments up to high temperatures. However, the lattice parameters of these samples were slightly different compared with the as-prepared samples (see Table 1). In addition, the anomalies corresponding to the orbital-order transition changed significantly their intensity and position after heating above 740 K (Figure 3a). These facts may indicate that the oxygen content of these samples changed. The effect of substitution on the monoclinic-to-orthorhombic transition temperature (T_{str}) is different depending on the M atoms. In the case of M = Sc, T_{str} increases.[32] This behavior is in agreement with the fact that T_{str} of $BiScO_3$[34] is above 980 K.[26] The strong effect of substitution on T_{str} is found in $BiMn_{0.95}Ga_{0.05}O_3$, where T_{str} is 800 K compared with T_{str} = 768 K in $BiMnO_3$ (Figure 3a). In the case of M = Cr, T_{str} decreases (T_{str} = 738 K for $BiMn_{0.85}Cr_{0.15}O_3$; Figure 3b). This behavior is in agreement with the fact that T_{str} of $BiCrO_3$ is 420 K.[33]

Figures 4 and 5 show magnetic susceptibilities of $BiMn_{1-x}M_xO_3$ between 2 and 150 K. The magnetic transition

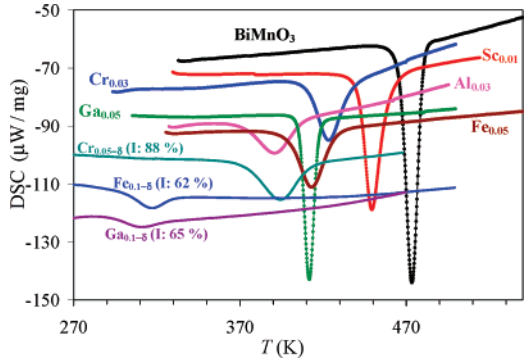

Figure 2. DSC curves of $BiMn_{1-x}M_xO_3$ containing monoclinic phase I. The samples are marked by "M_x". The curves on heating are shown. In the case of the two-phased samples containing phases I and II, the mass fraction of phase I is given and the composition of phase I is written as "$M_{x-\delta}$".

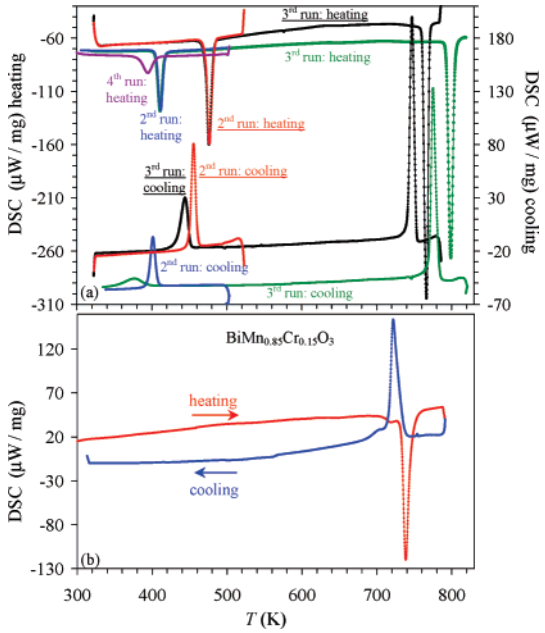

Figure 3. (a) DSC curves of $BiMnO_3$ and $BiMn_{0.95}Ga_{0.05}O_3$ on cycling. The second and forth runs are up to 520 K, and the third run is up to 790 K for $BiMnO_3$ and 823 K for $BiMn_{0.95}Ga_{0.05}O_3$. The curve legends for $BiMnO_3$ are underlined. Note that there is no different between the second and third runs on heating below 520 K but there is a large difference on cooling. (b) DSC curves of $BiMn_{0.85}Cr_{0.15}O_3$ on heating and cooling.

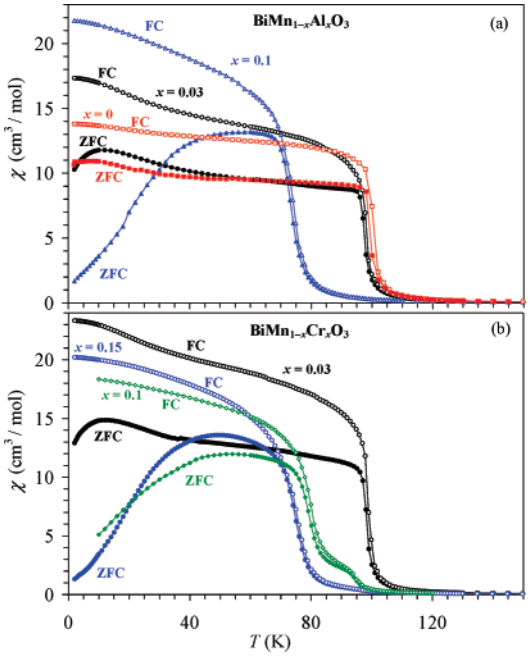

Figure 4. ZFC and FC dc magnetic susceptibility ($\chi = M/H$) curves of (a) $BiMn_{1-x}Al_xO_3$ ($x = 0$, 0.03, and 0.1) and (b) $BiMn_{1-x}Cr_xO_3$ ($x = 0.03$, 0.1, and 0.15) measured at 100 Oe. The curves between 2 and 150 K are shown.

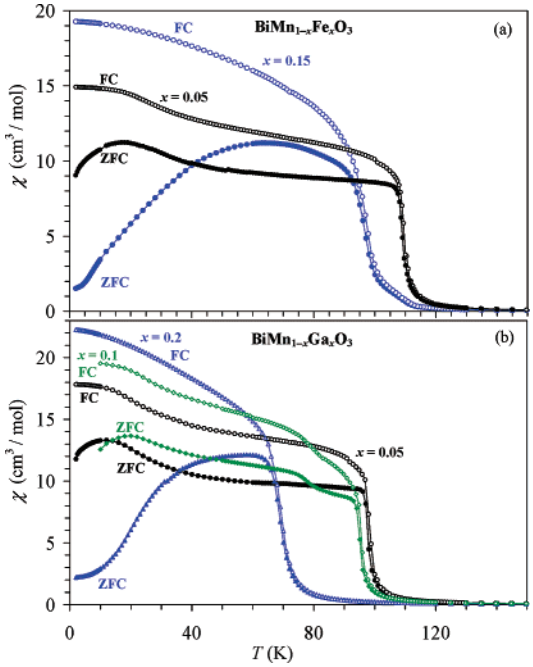

Figure 5. ZFC and FC dc magnetic susceptibility curves of (a) $BiMn_{1-x}Fe_xO_3$ ($x = 0.05$ and 0.15) and (b) $BiMn_{1-x}Ga_xO_3$ ($x = 0.05$, 0.1, and 0.2) measured at 100 Oe. The curves between 2 and 150 K are shown.

temperatures (T_C) were defined by the peak on the FC d(χT)/dT vs T curve and summarized in Table 3. The inverse ZFC magnetic susceptibilities (Figure 6) between 200 and 300 K were fit by the Curie−Weiss equation

$$\chi(T) = \mu^2_{\text{eff}} N(3k_B(T - \Theta))^{-1} \qquad (1)$$

where μ_{eff} is effective magnetic moment, N is Avogadro's number, k_B is Boltzmann's constant, and Θ is the Weiss constant. The fitting parameters are given in Table 3. It is interesting to note that the Weiss constants are almost the same in samples containing only phase I.

Figure 7 depicts the isothermal magnetization curves at 5 K. The coercive field (H_c) and the remnant magnetization (M_r) increase with increasing the content of M atoms. The H_c and M_r values and the magnetic moment at 5 K and 50 kOe (M_S) are reported in Table 3. The H_c and M_r parameters of phases II demonstrate drastic increase by about 1 order of magnitude compared with those of phases I. Note that the first magnetization curves from 0 to 50 kOe are not inside the hysteresis loops but slightly lower than the curves measured from 50 to −50 kOe and from −50 to 50 kOe. The M_S values of $BiMn_{1-x}M_xO_3$ with nonmagnetic M atoms (M = Al, Sc, Ga; $0 \le x \le 0.2$) are within the range of 3.7−3.9 μ_B/Mn that is close to the fully aligned spin value of 4 μ_B for Mn^{3+}. However, in the case of magnetic substitutions Cr^{3+} and Fe^{3+}, the M_S values are noticeably suppressed. This reduction of M_S can be explained if we assume that Fe^{3+} ($S = 5/2$, S is spin) and Cr^{3+} ($S = 3/2$) ions are coupled antiferromagnetically with surrounding Mn^{3+} and M^{3+} ions. The calculated M_S values are 2.65 μ_B/formula unit of $BiMn_{0.85}Fe_{0.15}O_3$ and 2.95 μ_B/formula unit of $BiMn_{0.85}Cr_{0.15}O_3$ that is very close to the experimental M_S values of 2.55 and 2.92 μ_B, respectively. Therefore, $BiMn_{1-x}M_xO_3$ with magnetic M atoms can be considered as random ferrimagnets.

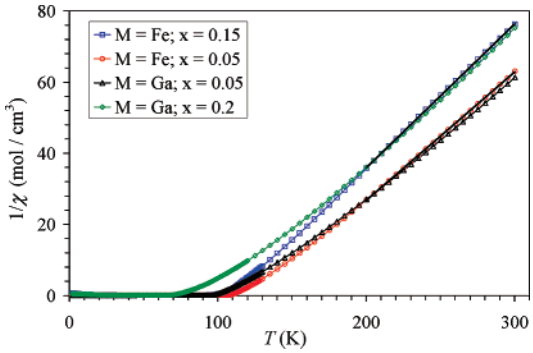

Figure 6. Inverse ZFC curves of $BiMn_{1-x}Fe_xO_3$ ($x = 0.05$ and 0.15) and $BiMn_{1-x}Ga_xO_3$ ($x = 0.05$ and 0.2). The Curie−Weiss fits between 200 and 300 K are shown by bold lines for $BiMn_{1-x}Fe_xO_3$.

The effective magnetic moments of $BiMn_{1-x}M_xO_3$ with nonmagnetic M atoms are slightly larger than the calculated ones (Table 3). However, the effective magnetic moments are smaller than the calculated ones in the case of $BiMn_{1-x}M_xO_3$ with M = Cr and Fe. It is noticeable especially for $BiMn_{0.85}Fe_{0.15}O_3$ (4.45 μ_B (expt) vs 5.07 μ_B (calcd)). The value of 4.45 μ_B is close to the magnetic moment in the case of substitution with nonmagnetic M^{3+} ions. We can explain this fact if we assume that the antiferromagnetic interaction of Fe^{3+} ions with surrounding ions is so strong that even at RT magnetic moments of Fe^{3+} ions have no contribution (similar to the formation of spin-singlet states). In this context, we note that $BiFeO_3$ is an antiferromagnet with the large Neél temperature of about 640 K.[36]

(36) Wang, J.; Neaton, J. B.; Zheng, H.; Nagarajan, V.; Ogale, S. B.; Liu, B.; Viehland, D.; Vaithyanathan, V.; Schlom, D. G.; Waghmare, U. V.; Spaldin, N. A.; Rabe, K. M.; Wuttig, M.; Ramesh, R. *Science* **2003**, *299*, 1719.

Table 3. Different Parameters Deduced from the Magnetization Curves of $BiMn_{1-x}M_xO_3$[a]

M	x	μ_{eff} (μ_B)	μ_{cal} (μ_B)	Θ (K)	T_C (K)	H_c (Oe)	M_r (μ_B)	M_S (μ_B)
	0[32]	4.93	4.90	123	102	3	0.013	3.92
Al	**0.03**	4.88	4.83	122	99	30	0.095	3.62
Al	0.10	4.79	4.65	112	75	192	0.500	3.45
Sc	**0.01**	4.93	4.88	123	100	9	0.031	3.77
Sc	*0.05*[32]	4.84	4.78	112	97 (I), 78 (II)	70	0.260	3.58
Sc	0.10[32]	4.68	4.65	107	70	144	0.385	3.34
Cr	**0.03**	4.82	4.87	122	99	18	0.079	3.55
Cr	*0.05*	-		-	98 (I), - - (II)	32	0.064	3.38
Cr	*0.10*	-		-	96 (I), 81 (II)	92	0.303	3.17
Cr	0.15	4.68	4.76	107	76	195	0.568	2.92
Fe	**0.05**	4.71	4.96	126	110	24	0.069	3.35
Fe	*0.10*	-		-	112 (I), 98 (II)	-	-	-
Fe	0.15	4.45	5.07	111	98	173	0.564	2.55
Ga	**0.05**	4.83	4.78	122	99	10	0.033	3.71
Ga	*0.10*	4.75	4.65	121	96 (I), 81 (II)	-	-	-
Ga	0.20	4.52	4.38	109	70	355	0.877	3.02

[a] T_C is defined by the peak on the FC $d\chi T/dT$ vs T curve. μ_{eff} and Θ are determined by the Curie−Weiss fit of the inverse ZFC χ vs T curves between 200 and 300 K. H_c is the coercive field, M_r is the remnant magnetization, and M_S is the magnetization at 5 K and 50 kOe. All the values are given per mol of a sample or per formula unit (fu). The compositions marked by bold x are in the orbital-ordered state (phase I); the compositions marked by italic x contained two phases (I and II). Key: "-" means the data were not measured; "- -" means out of detection limit; I is for phase I; II is for phase II.

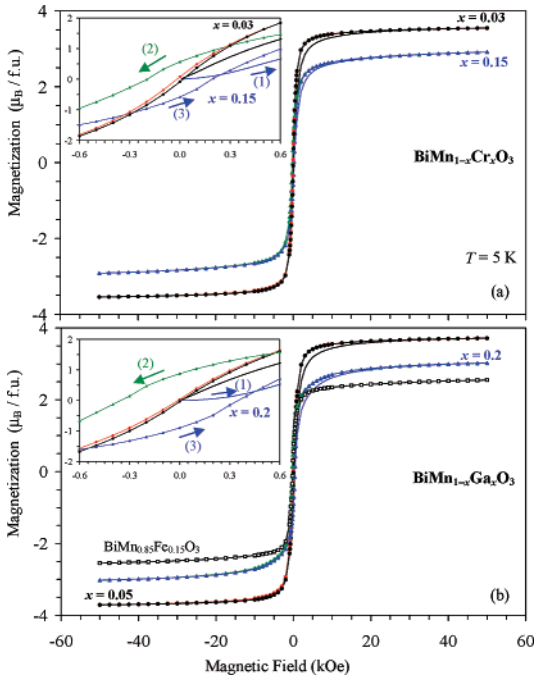

Figure 7. Isothermal magnetization curves at 5 K for (a) $BiMn_{1-x}Cr_xO_3$ ($x = 0.03$ and 0.15) and (b) $BiMn_{1-x}Ga_xO_3$ ($x = 0.05$ and 0.2) and $BiMn_{0.85}Fe_{0.15}O_3$. (Only the curve measured from 50 to −50 kOe is shown). Insets show the enlarge curves between −0.6 and 0.6 kOe for $BiMn_{1-x}Cr_xO_3$ and $BiMn_{1-x}Ga_xO_3$: (1) run from 0 to 50 kOe; (2) run from 50 to −50 kOe; (3) run from −50 to 50 kOe.

The ZFC curves of samples with the phase I and II structures are quite different (Figures 4 and 5). In phases I, the ZFC curves show a small hump at low temperatures, and then they are almost constant in a wide temperature range below T_C. This behavior is typical for a soft ferromagnet. In phases II, the ZFC curves demonstrate very broad maxima typical for cluster-glass-like or spin-glass-like materials. The difference in behavior depends only on the crystal structure (the orbital-ordered or orbital-disordered structure), and it does not depend on the x value. For example, $BiMn_{0.95}Ga_{0.05}O_3$ (phase I) and $BiMn_{0.95}Sc_{0.05}O_3$ (97% of phase II)[32] show different behavior.

In phase I, the ferromagnetic transition temperature T_C slightly decreases on substitution for M = Al, Sc, Cr, and Ga compared with $BiMnO_3$. The exception is the $BiMn_{1-x}Fe_xO_3$ system where T_C increases in phase I (Figure 5a). In all the systems, T_C drops by 10−20 K as soon as we have phase II. The rather sudden drop of T_C in phases II gives support that orbital order enhances the magnetic interactions in phases I and increases T_C. A small upturn on the χ vs T curve of $BiMn_{0.85}Fe_{0.15}O_3$ was observed below 110 K. This observation can be explained by inhomogeneous distribution of Fe atoms or traces of phase I even though only one monoclinic phase II was detected by XRD.

In conclusion, effects of substitution in the Mn sublattice of $BiMnO_3$ were investigated by differential scanning calorimetry and magnetization measurements. The orbital order of $BiMnO_3$ was found to be very fragile, and the temperature of orbital ordering was very sensitive to substitution. The ferromagnetic temperature in the orbital-ordered state was only slightly affected. Ferromagnetic cluster-glass-like behavior was found in the orbital-disordered state.

Supporting Information Available: XRD patterns of the as-prepared $BiMn_{0.97}Cr_{0.03}O_3$ and after the DSC experiment up to 823 K (Figure S1), XRD patterns of the as-prepared $BiMn_{0.97}Al_{0.03}O_3$ and after the DSC experiment up to 810 K (Figure S2), the detailed DSC curves of some samples (Figures S3−5), and the M vs H curves of $BiMn_{0.85}Fe_{0.15}O_3$ (Figure S6) (PDF). This material is available free of charge via the Internet at http://pubs.acs.org.

IC0701615

(37) Izumi, F.; Ikeda, T. *Mater. Sci. Forum* **2000**, *321*−*324*, 198.